NASA
TN
D-7974
c.1

NASA TECHNICAL NOTE

NASA TN D-7974

NASA TN D-7974

2.4/4

LOAN COPY: RETU
AFWL TECHNICAL L
KIRTLAND AFB, I

4.

VIKING ENTRY VEHICLE AERODYNAMICS AT M = 2 IN AIR AND SOME PRELIMINARY TEST DATA FOR FLIGHT IN CO_2 AT M = 11

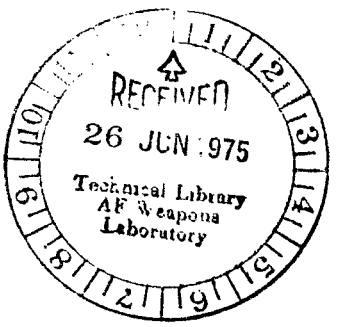

Robert I. Sammonds and Robert L. Kruse

Ames Research Center
Moffett Field, Calif. 94035

3.

NATIONAL AERONAUTICS AND SPACE ADMINISTRATION • WASHINGTON, D. C. • JUNE 1975

5.

TECH LIBRARY KAFB, NM

0133533

1. Report No.	2. Government Accession No.	3. Recipient's Catalog No.
NASA TN D-7974		

4. Title and Subtitle

VIKING ENTRY VEHICLE AERODYNAMICS AT $M = 2$ IN AIR AND SOME PRELIMINARY TEST DATA FOR FLIGHT IN CO_2 AT $M = 11$

5. Report Date: June 1975

6. Performing Organization Code:

7. Author(s)

Robert I. Sammonds and Robert L. Kruse

8. Performing Organization Report No.: A-4825

10. Work Unit No.: 185-47-68-01

9. Performing Organization Name and Address

Ames Research Center
Moffett Field, Calif. 94035

11. Contract or Grant No.:

13. Type of Report and Period Covered: Technical Note

12. Sponsoring Agency Name and Address

National Aeronautics and Space Administration
Washington, D. C. 20546

14. Sponsoring Agency Code:

15. Supplementary Notes

16. Abstract

The static and dynamic aerodynamic characteristics of the Viking Entry Vehicle have been determined experimentally in free flight in air at a Mach number near 2. Preliminary results have also been obtained in CO_2 at $M_\infty = 11$. The low speed tests in air confirmed a region of dynamic instability previously observed at the Arnold Engineering Development Center (AEDC). The instability was greatest at the smallest pitch amplitudes but decreased with increasing amplitude until a limit cycle was reached at about 8°. The tests in CO_2 indicated increased drag coefficients of 3 percent with respect to those in air. Errors in the drag coefficient of this magnitude would significantly affect the reconstruction of the Martian atmosphere during entry of the Viking spacecraft.

17. Key Words (Suggested by Author(s))

Large angle spherically blunted cones
Atmospheric entry vehicles
Mars probe-lander configuration
Hypersonic aerodynamics of large angle blunted cones
Blunt cones
Dynamic stability
Static stability
Ballistic range test
Tests in CO_2 atmosphere

18. Distribution Statement

Unclassified – Unlimited

STAR Categories – 02

19. Security Classif. (of this report)	20. Security Classif. (of this page)	21. No. of Pages	22. Price*
Unclassified	Unclassified	26	$3.75

*For sale by the National Technical Information Service, Springfield, Virginia 22151

SYMBOLS

A	reference area, maximum body cross-sectional area, cm^2
C_D	drag coefficient, $\frac{\text{drag}}{q_\infty A}$
C_L	lift coefficient, $\frac{\text{lift}}{q_\infty A}$
C_{L_α}	lift-curve slope, per rad
C_{m_α}	pitching-moment-curve slope (based on linear pitching-moment curve), per rad
$C_{m_q} + C_{m_{\dot{\alpha}}}$	damping-in-pitch derivative, $\frac{\partial C_m}{\partial(qd/V)} + \frac{\partial C_m}{\partial(\dot{\alpha}d/V)}$, per rad
d	reference diameter, maximum body diameter, cm
I_x	moment of inertia about the roll axis, $g\text{-}cm^2$
I_y	moment of inertia about transverse axis through center of gravity, $g\text{-}cm^2$
M	Mach number
m	model mass, g
n	number of data points
p	static pressure, mmHg
q	angular pitching velocity, rad/sec
q_∞	free-stream dynamic pressure, N/m^2
Re_d	Reynolds number based on free-stream gas properties and model reference diameter, d
r	radius of curvature of rounded corners and cone apex, cm
$S.D.$	standard deviation, $\left(\frac{1}{n} \Sigma \epsilon^2\right)^{1/2}$
V	velocity of the model with respect to the atmosphere, km/sec
x,y,z	earth-fixed axes; also displacements along these axes, cm
$\overline{x}$	axial distance from model nose to center-of-gravity location, cm
$\overline{z}$	transverse distance from model axis of symmetry to center-of-gravity position, cm

α angle of attack (angle, projected onto the xz plane, between model longitudinal axis and the stream direction), deg

α_m average value of maximum-angle envelope with respect to the trim angle of attack, deg

α_{min} average value of minimum-angle envelope with respect to the trim angle of attack, deg

α_{rms} root-mean-square resultant angle of attack, $\left(\frac{\int_0^x \bar{\alpha}_r^2 \, dx}{x}\right)^{1/2}$, deg

$\bar{\alpha}_r$ resultant angle of attack, $\tan^{-1}\sqrt{\tan^2 \alpha + \tan^2 \beta}$, deg

α_t resultant trim angle of attack, deg

β angle of sideslip (angle, projected onto the xy plane, between model axis of symmetry and the stream direction), deg

ϵ deviation of the measured results from a fitted curve or a mean value

ξ dynamic-stability parameter, $C_D - C_{L_\alpha} + \left(C_{m_q} + C_{m_{\dot{\alpha}}}\right)\left(\frac{d}{\sigma}\right)^2$

ρ free-stream density, g/cm^3

σ transverse radius of gyration with respect to the center of gravity of the model, $(I_y/m)^{1/2}$, cm

$(\dot{})$ first derivative with respect to time

Subscripts

b base

c corner

n nose

∞ free-stream conditions

VIKING ENTRY VEHICLE AERODYNAMICS AT $M = 2$ IN AIR AND SOME PRELIMINARY TEST DATA FOR FLIGHT IN CO_2 AT $M = 11$

Robert I. Sammonds and Robert L. Kruse

Ames Research Center

SUMMARY

The static and dynamic aerodynamic characteristics of the Viking Entry Vehicle have been determined experimentally in free flight in air at a Mach number near 2. Preliminary results have also been obtained in CO_2 at $M_\infty = 11$. The low speed tests in air confirmed a region of dynamic instability previously observed at the Arnold Engineering Development Center (AEDC). The instability was greatest at the smallest pitch amplitudes but decreased with increasing amplitude until a limit cycle was reached at about 8°. The tests in CO_2 indicated increased drag coefficients of 3 percent with respect to those in air. Errors in the drag coefficient of this magnitude would significantly affect the reconstruction of the Martian atmosphere during entry of the Viking spacecraft.

INTRODUCTION

Aerodynamic data applicable to the Viking entry configuration are available in references 1–13 for a wide range of test conditions. Among these, ballistic range data (refs. 1 and 2) have shown configurations of this general shape to be dynamically unstable in the transonic speed range. This region of dynamic instability was later confirmed in forced oscillation tests conducted at the Arnold Engineering Development Center (ref. 4). These same forced oscillation tests also showed a second region of instability near a Mach number of 2, unconfirmed by ballistic range tests. Since these instabilities can have a significant detrimental effect on vehicle flight behavior, it was believed desirable to further examine and confirm the instability at $M = 2$ in free flight tests.

In addition, at the start of this test program, most of the available aerodynamic data for Viking had been obtained in air as a test medium. Some tests were being conducted concurrently with the present program in tetrafluoromethane, CF_4 (refs. 2, 3, and unpublished data from Martin-Marietta Corp., Denver Division). Since the Martian atmosphere is composed mainly of carbon dioxide, it was felt that a preliminary investigation should be conducted to determine the effects, if any, of operating in a CO_2 atmosphere. For these tests, matching of the equilibrium composition of the gas in the shock layer was emphasized rather than matching of selected nonequilibrium flow conditions. The latter would also be of interest, but they are not considered here.

The tests reported herein were conducted in free flight through air and CO_2 in the ballistic range facilities of Ames Research Center.

MODELS

For these tests, two versions of the Viking Entry Vehicle were used. These models were geometrically identical to a location 0.333 d aft of the physical nose, but had different base cover geometry (fig. 1(a)). The forebodies consisted of a 70° half-angle cone with the apex rounded to a radius of 0.25 d and with the corner slightly rounded. The afterbodies consisted of two truncated conical segments with the half-angles shown in figure 1(a).

Model A, which had the shorter afterbody, is identical to configuration 721M reported in reference 4. This particular configuration was selected, for convenience, because it allowed the use of a homogeneous model with the proper center-of-gravity location ($\bar{x}/d$ = 21.3 percent) but still showed the dynamic stability characteristics of interest.

Model B was made bimetallic (fig. 1(b)) in order to locate the longitudinal center of gravity ($\bar{x}/d$) at 21.5 percent from the physical nose and the lateral center of gravity ($\bar{z}/d$) at 1.34 percent from the axis of symmetry to achieve a desired trim angle of attack of 11.2° (ref. 7).

TESTS

The models were tested in free flight – model A in the Ames Pressurized Ballistic Range (PBR) and model B in the Ames Hypervelocity Free-Flight Aerodynamic Facility (Aero). Model A was tested in air at Mach numbers near 2.0 and Reynolds numbers (based on model diameter) of about 600,000.

Model B was tested in CO_2 at a Mach number of 11.3 ($\approx$ 3 km/sec), a Reynolds number (based on model diameter) of 890,000, and an equilibrium density ratio (ρ/ρ_∞) across a normal shock wave of 10^{-1}. These conditions were selected so that the equilibrium composition of the gas in the shock layer would approximate that for the full-scale vehicle while, at the same time, the Reynolds number would represent a point on the Viking nominal entry trajectory. (It was also determined that the ambient density would be sufficient to give the desired model pitching motion.) Chemical analysis of gas samples taken from the test facility immediately before model launch showed a mixture composition of roughly 0.99 CO_2, 0.008 N_2, and 0.002 O_2.

Model A was launched from a 57-mm smooth-bore powder gas gun; model B was launched from a 38.1-mm (1.5 in.) diameter deformable-piston, light-gas gun (ref. 14). The models were, in each case, adapted to the guns by means of four-piece plastic sabots. Figure 2 is a photograph of model A in a typical four-piece nylon sabot. Model B, launched at higher speeds, used a four-piece polycarbonate (Lexan) sabot. The sabots launched the model at both 0° angle of attack (fig. 2) and at 10° angle of attack using a canted sabot (not shown).

Shadowgraphs were obtained in orthogonal planes at 16 observation stations over a ballistic flight of 23 m (Aero) and at 24 observation stations over a ballistic flight of 62 m (PBR). The photographic observation stations for each facility contain accurately calibrated fiducial systems so that the spatial position and attitude of the model at each station can be determined precisely over the entire length of the flight. Electronic chronographs measured the time of the model flight between stations.

Accuracy of the Data

The accuracies of the measured quantities for obtaining the aerodynamic coefficients from the model motions are as follows:

Measurement	PBR	Aero
x, y, z	±0.013 cm	±0.013 cm
α, β	±0.125°	±0.5°
t	0.625 μsec	0.02 μsec
p_∞	0.1 mm Hg	0.1 mm Hg

REDUCTION OF THE DATA

The aerodynamic coefficients were determined from analysis of the free-flight motions by use of the data reduction program described in reference 15. This program determines drag from the time-distance history of each flight, the static and dynamic stabilities from the oscillatory history of model motion, and the lift-curve slope from the swerve measurements and oscillatory motion of the model.

Linear aerodynamics are assumed in the data reduction program. However, this does not prevent the use of the method for bodies with nonlinear stability coefficients, since a method for defining the nonlinear coefficients from the quasi-linear data analysis is available (refs. 15 and 16), and was applied.

Although the data reduction program is theoretically restricted to models having only small asymmetries, past experience has shown that reasonably reliable results can be expected for models having significant amounts of asymmetry. This will be discussed in greater detail in the Results and Discussion section with regards to the CO_2 tests of the trimmed model.

RESULTS AND DISCUSSION

The static and dynamic characteristics of the Viking configuration for the two series of tests incorporated here are presented in table 1 and in figures 3 through 10. Figures 3 through 9 show data for the low-speed tests in air, while figure 10 presents the drag coefficients for the high-speed tests in CO_2.

Tests in Air at $M = 2$

The experimentally determined dynamic-stability coefficients ($C_{m_q} + C_{m_{\dot{\alpha}}}$) for model A are presented in figure 3. Included in this figure for comparison is a faired curve representing the data

shown in figure 13(a) of reference 4. Although there appears to be considerable scatter in the data, a close examination shows a definite variation with pitching amplitude. This variation of the dynamic stability with pitching amplitude is shown more clearly in figure 4, which is a crossplot of figure 3 as a function of pitching amplitude for $M = 2.1$ (the point where the AEDC data showed a maximum instability). This presentation shows the model to be dynamically unstable at the lower pitching amplitudes, but stable above an amplitude of about 8°. At small angles of attack in the $M = 1.9$ to 2.3 range (fig. 3), the model is dynamically unstable as indicated by the data of reference 4. Also, at Mach numbers above 2.7, the ballistic range data show dynamic stability even at pitch amplitudes as low as 2°. Although the AEDC data appear in general to show more instability than the ballistic range data, note that the pitch amplitudes for the AEDC tests were less than 2°. At these amplitudes, the data from reference 4 would agree well with a reasonable extrapolation of the present data (fig. 4).

The quasi-linear pitching-moment and lift-curve slopes (C_{m_α} and C_{L_α}, respectively) are presented in figures 5 and 6, respectively, as a function of Mach number and pitch amplitude. Both the static stability (C_{m_α}) and the lift-curve slopes (C_{L_α}) are relatively independent of Mach number in this speed range. The model is statically stable but the stability decreases moderately with increasing pitch amplitude (fig. 5(b)). The lift-curve slope is negative and is relatively unaffected by pitch amplitude.

The nonlinear pitching moment and lift curves derived from the above C_{m_α} and C_{L_α} data by the methods of references 15 and 16 are presented in figures 7 and 8, respectively. These data are presented for two-term representations of the nonlinear curves, one being a linear plus a squared term, and the other a linear plus a cubic term. The two curves are in both cases, identical up to 12° angle of attack. Ticks indicate both the maximum test values of α_{rms} and pitch amplitude. The tick for the maximum pitch amplitude should be considered the absolute limit to which the curves can be used. On comparison of these moment and lift curves with existing wind-tunnel data, the ballistic data are seen to indicate somewhat less stability than the wind-tunnel data reported in reference 12, although both sets of data show the same degree and type of nonlinearity. The lift data from this test are essentially identical to that reported in reference 6 and indicate only a small amount of nonlinearity. It should be pointed out that, due to the nonlinearity of the pitching-moment curve (fig. 7), the deduced values of $C_{m_q} + C_{m_{\dot\alpha}}$ presented in figure 3 are slightly high. A detailed discussion of this effect is given in reference 16.

The drag coefficients obtained for model A are presented in figure 9. The data show little effect of either Mach number or angle of attack for the ranges of these variables encountered during the tests. The agreement between these data and that of reference 6 is excellent, within 0.7 percent.

Tests in CO_2 at $M = 11.3$

The aerodynamic data obtained for model B in a simulated Martian atmosphere (CO_2) are presented in table 1 and in figure 10. This series of tests was exploratory in nature, intended to provide a preliminary look into possible effects of flight in CO_2 on the aerodynamic characteristics of the Viking entry vehicle. The majority of the data is presented in tabulated form in table 1 because of difficulties encountered in presenting the data graphically, as discussed below.

The drag coefficients obtained for model B are presented, however, in figure 10. Also included in this figure are data from references 2, 3, 12, 13, and unpublished data from the Martin-Marietta Corp., Denver Division (CF_4), and the Ames Hypervelocity Free-Flight Aerodynamic Facility (air). Note that the data presented in reference 12 are a compilation of data presented in references 5, 6, 9, and 10, and are (in general) for configurations with flat afterbodies. The configuration of references 3, 13, and the unpublished Martin-Marietta data, however, had the Viking afterbody. Although there are variations in M and Re among the data compared, data for the PAET configuration (ref. 17) show only small decreases in drag coefficient at $M > 8$ and only a small effect of Reynolds number for $Re_d > 400{,}000$. It can be seen that in general the results in CO_2 and CF_4 are slightly higher than those in air. The data from the tests in CO_2 compared with the unpublished Ames data in air show an increase in C_D of approximately 3 percent in this angle range. The data of references 12 and 13 agree closely with the unpublished Ames data for tests in air. The data of references 2 and 3 show considerable differences between the results in air and CF_4, while the unpublished Martin-Marietta data show a difference comparable to that between the data of this report and the unpublished Ames data. This is significant because errors in drag of this magnitude would appreciably affect the atmospheric reconstruction to be performed from data taken during entry. As a result, it would be desirable to obtain drag coefficients for other Mach numbers along the entry trajectory.

For the other aerodynamic properties, limitations to small asymmetry in the data reduction program (refs. 15 and 16) are significant since the trim angle here is about 11°. As noted earlier, past experience has shown that reasonably reliable results are obtained for models having significant amounts of asymmetry. However, for normal symmetric models, where the oscillatory motion is about zero angle of attack, the average value of the maximum-angle envelope (α_m) is representative of the model motion. For the asymmetric model this is no longer true because the model now oscillates about its trim angle of attack. Thus, the average value of the maximum-angle envelope (α_m) deduced by the data reduction program is referenced to the trim angle and does not clearly represent the model motion. Because of uncertainties in how to present these data graphically and because of the preliminary nature of the data it was decided to present these data in tabular form only. However, even though there are uncertainties regarding the interpretation of the data, there are some observations that can be made. The data show the model to be both statically and dynamically stable, and to have a negative lift-curve slope, as expected for this type of blunt body. Both the static-stability coefficients (C_{m_α}) and the lift-curve slopes (C_{L_α}) decrease with increasing pitch amplitude. (An exception to this observation is the static-stability coefficient for the model motion having the smallest pitch amplitude. No explanation is available for this apparent anomaly.) The dynamic-stability coefficients appear to be in generally good agreement with configurations of this general class (ref. 11).

It is clear that further tests in CO_2 to establish L/D, α_t, and other significant properties of the Viking entry vehicle would be warranted.

CONCLUDING REMARKS

The aerodynamic data presented here show the results of tests to evaluate the dynamic stability characteristics of the Viking Entry Probe at $M \approx 2$ in air and of preliminary tests to evaluate the effect of a simulated Martian atmosphere on the vehicle.

The dynamic-stability data ($C_{m_q} + C_{m_{\dot{\alpha}}}$) obtained at low speed in air confirm the region of dynamic instability at Mach numbers near 2 previously seen in forced oscillation tests at AEDC (ref. 4). Agreement between these two sets of data is quite good.

The static-stability data obtained from ballistic-range tests in air show the model to be somewhat less stable than do the wind-tunnel data of reference 12 although both sets of data show that the static stability decreases moderately with increasing pitch amplitude.

The lift coefficients obtained from the ballistic range tests in air are essentially identical to the wind-tunnel data presented in reference 6 and relatively unaffected by Mach number and pitch amplitude.

A significant effect of the simulated Martian atmosphere is an increase in the drag coefficient of 3 percent. Errors in drag of this magnitude would appreciably affect atmospheric reconstruction during entry and should be investigated in more detail. The model was statically and dynamically stable with no apparent anomalies that can be attributed to the test medium (CO_2).

Ames Research Center
National Aeronautics and Space Administration
Moffett Field, Calif. 94035, November 11, 1974

REFERENCES

1. Sammonds, Robert I.: Dynamics of High-Drag Probe Shapes at Transonic Speeds. NASA TN D-6489, 1971.

2. Krumins, Maigonis: Drag and Stability of Various Mars Entry Configurations. IAF Paper RE138, Oct. 1968. 19th Congress of the International Astronautical Federation, New York.

3. Hunt, James L.; Jones, Robert A.; and Midden, Raymond E.: Simulation of Real-Gas Effects for Mars Entry. J. Spacecraft. Vol. 11, No. 1.

4. Uselton, B. L.; Shadow, T. O.; and Mansfield, A. C.: Damping-in-Pitch Derivatives of 120- and 140-Degree Blunted Cones at Mach Numbers from 0.6 Through 3. AEDC-TR-70-49, 1970.

5. Campbell, James F.; and Howell, Dorothy T.: Supersonic Aerodynamics of Large-Angle Cones. NASA TN D-4719, 1968.

6. Campbell, James F.: Supersonic Aerodynamic Characteristics and Shock Standoff Distances for Large-Angle Cones With and Without Cylindrical Afterbodies. NASA TN D-5334, 1969.

7. Campbell, James F.; and Howell, Dorothy T.: Supersonic Lifting Capabilities of Large-Angle Cones. NASA TN D-5499. 1969.

8. Nichols, James O.; and Nierengarten, Edward A: Aerodynamic Characteristics of Blunt Bodies. JPL TR 32-677, 1964.

9. Walker, Billy; and Weaver, Robert W.: Static Aerodynamic Characteristics of Blunted Cones in the Mach Number Range from 2.2 to 9.5. JPL TR 32-1213. 1967.

10. Marko, Wayne J.: Static Aerodynamic Characteristics of Three Blunted Sixty-Degree Half-Angle Cones at Mach Numbers from 0.6 to 1.30. JPL TR 32-1298. 1968.

11. Sammonds, Robert I.: Aerodynamics of Mars Entry Probe-Lander Configurations at a Mach Number of 10. NASA TN D-5608, 1970.

12. Click, B. F.: Aerodynamic Data Book (VER-10). TR-3709014, Martin-Marietta Corp., Denver Div. 1970.

13. Goldberg, Theodore J.; and Emery, James C.: Longitudinal Aerodynamic Characteristics of the Viking Lander Capsule at Mach 6. NASA TM X-2205, 1970.

14. Canning, T. N.; Seiff, A.; and James, C. S.: editors, Ballistic Range Technology, AGARDograph 138, Ch. 2, August, 1970.

15. Malcolm, Gerald N.; and Chapman, Gary T.: A Computer Program for Systematically Analyzing Free-Flight Data to Determine the Aerodynamics of Axisymmetric Bodies. NASA TN D-4766, 1968.

16. Canning, T. N.; Seiff, A.; and James, C. S.: editors, Ballistic Range Technology, AGARDograph 138, Ch. 7. Aug. 1970.

17. Sammonds, Robert I.; and Kruse, Robert L.: Aerodynamic Characteristics of the Planetary Atmosphere Experiments Test Entry Probe. J. Spacecraft, vol. 12, no. 1, Jan. 1975, pp. 22–27.

TABLE 1. – DATA SUMMARY

Run	M_∞	$Re \times 10^{-6}$	Station Interval	C_D	$-C_{m_\alpha}$, per rad	$-C_{L_\alpha}$, per rad	ξ	$C_{m_q}+C_{m_{\dot\alpha}}$, per rad	$\rho_\infty \times 10^3$, g/cm^3	α_{rms}, deg	α_m, deg	α_m/α_{min}	α,β deviation, deg	y,z deviation, cm	diameter, cm	$m \times 10^{-2}$, gm	$I_y \times 10^{-2}$, g-cm^2	I_y/I_x	md^2/I_y	$\frac{\rho_\infty A}{2m} \times 10^3$, cm^{-1}	α_t, deg	V_∞, km/sec
(a) Aerodynamic facility																						
902	1.89	0.5423	1-9	1.573	0.124	1.44	5.14	0.11	0.2999	2.68	3.88	129.33	0.40	0.018	5.0833	0.2498	0.3219	0.5754	20.0570	0.1218		
	1.76	.5042	3-12	1.562	.123	1.41	2.00	−.05		3.09	4.21	70.16	.40	.021								
	1.61	.4624	6-15	1.546	.117	1.53	4.34	.06		3.11	4.58	65.43	.55	.022								
	1.57	.4494	7-16	1.542	.112	1.56	5.56	.12		3.52	4.81	68.71	.49	.019								
903	1.92	.5498	1-10	1.580	.109	1.49	.92	−.11	.3003	5.07	7.35	7.42	.59	.015	5.0765	.2489	.3195	.5757	20.0754	.1221		
	1.81	.5184	3-12	1.573	.110	1.48	.48	−.13		5.28	7.32	5.71	.56	.037								
	1.63	.4682	6-16	1.555	.112	1.50	3.18	.01		5.42	8.04	9.13	.73	.028								
904	2.26	.6527	1-10	1.586	.117	1.56	6.82	.18	.3018	3.07	3.51	1.34	.45	.014	5.0818	.2499	.3221	.5751	20.0385	.1224		
	2.13	.6151	3-12	1.583	.115	1.40	7.73	.24		3.62	4.18	1.31	.49	.023								
	1.92	.5550	6-16	1.572	.115	1.53	7.31	.21		4.58	5.11	1.22	.56	.042								
905	3.10	.9047	1-10	1.574	.127	1.52	.07	−.15	.3043	1.38	1.88	5.37	.36	.021	5.0726	.2494	.3209	.5753	20.0033	.1233		
	2.92	.8526	3-12	1.574	.125	1.47	2.00	−.05		1.27	1.83	6.77	.40	.031								
	2.76	.8036	5-14	1.576	.122	1.53	−1.51	−.23		1.29	1.86	10.94	.45	.027								
	2.60	.7574	7-16	1.578	.125	1.43	2.85	−.01		1.57	2.09	13.93	.51	.030								
906	2.40	.6958	1-10	1.578	.112	1.45	6.91	.19	.3029	2.89	3.90	2.76	.49	.023	5.0798	.2484	.3199	.5745	20.0416	.1235		
	2.26	.6556	3-12	1.575	.116	1.58	9.72	.33		3.38	4.57	2.34	.46	.034								
	2.13	.6179	5-14	1.573	.116	1.58	11.46	.42		4.06	5.42	2.16	.23	.030								
	2.01	.5825	7-16	1.570	.111	1.56	7.01	.19		4.59	5.72	1.94	.48	.038								
907	2.60	.7460	1-10	1.589	.111	1.45	6.25	.16	.3004	3.46	4.48	1.66	.47	.015	5.0785	.2493	.3212	.5763	20.0189	.1221		
	2.52	.7241	2-11	1.589	.108	1.46	5.18	.11		3.55	4.52	1.97	.50	.020								
	2.38	.6826	4-13	1.587	.111	1.46	4.52	.07		3.86	5.11	2.12	.51	.021								
	2.31	.6628	5-14	1.586	.111	1.41	4.89	.09		4.16	5.35	2.06	.49	.022								
	2.18	.6248	7-16	1.583	.116	1.49	4.84	.09		4.54	5.71	1.83	.51	.021								
(b) Pressurized ballistic range																						
1536	1.99	.5690	4-15	1.579	.105	1.43	2.25	−.04	.2993	7.22	9.42	3.02	.37	.019	5.0813	.9496	1.2320	.5726	19.8966	.0320		
	1.89	.5392	8-19	1.570	.105	1.39	1.66	−.07		7.29	9.65	2.47	.58	.030								
	1.80	.5138	11-22	1.566	.103	1.43	2.19	−.04		7.53	10.13	2.50	.55	.041								
	1.74	.4977	14-24	1.559	.102	1.44	4.42	.07		8.15	10.52	2.55	.66	.034								
1537	2.10	.6207	4-15	1.549	.102	1.46	.98	−.10	.3078	9.99	14.74	16.94	.23	.016	5.0813	.9493	1.2330	.5734	19.8778	.0329		
	2.02	.5991	7-18	1.547	.102	1.44	1.85	−.06		10.46	15.02	17.07	.24	.032								
	1.92	.5692	10-21	1.539	.102	1.44	1.65	−.07		10.45	15.47	15.63	.28	.034								
1538	2.10	.6284	3-13	1.560	.104	1.45	1.54	−.07	.3097	6.72	9.29	3.67	.45	.018	5.0818	.9502	1.2350	.5731	19.8719	.0331		
	2.00	.5965	7-18	1.552	.104	1.46	4.19	.06		7.05	9.88	3.92	.34	.016								
	1.93	.5756	9-20	1.547	.102	1.45	4.44	.07		7.22	10.36	3.98	.30	.017								
	1.84	.5495	12-23	1.550	.103	1.44	3.98	.05		7.76	11.05	3.97	.17	.022								
1539	2.08	.6281	4-14	1.558	.103	1.49	1.24	−.09	.3122	8.16	12.09	6.43	.10	.021	5.0823	.9451	1.2260	.5719	19.9161	.0335		
	2.01	.6075	7-17	1.559	.103	1.48	1.52	−.08		8.64	12.35	6.35	.09	.030								
	1.93	.5811	9-20	1.551	.103	1.48	2.24	−.04		8.67	12.97	6.31	.38	.033								
	1.84	.5543	12-23	1.551	.102	1.47	2.30	−.04		8.96	13.48	6.34	.50	.037								
	1.78	.5377	16-24	1.557	.101	1.43	2.72	−.01		9.16	13.85	6.63	.53	.041								
1540	2.15	.6348	3-13	1.564	.105	1.48	1.82	−.06	.3069	6.07	8.77	30.24	.10	.015	5.0818	.9492	1.2320	.5729	19.8917	.0328		
	2.06	.6077	7-17	1.566	.106	1.51	2.90	−.01		6.31	9.08	36.32	.15	.014								
	1.97	.5817	9-20	1.561	.107	1.51	1.35	−.09		6.25	9.29	29.97	.18	.014								
	1.88	.5553	12-23	1.561	.107	1.49	.08	−.15		6.39	9.36	34.67	.21	.014								
1556	2.25	.6721	3-14	1.555	.103	1.47	.92	−.11	.3092	7.84	11.51	8.53	.16	.028	5.0818	.9494	1.2340	.5720	19.8760	.0330		
	2.15	.6415	7-18	1.553	.102	1.47	1.31	−.09		7.95	11.67	9.26	.24	.038								
	2.08	.6191	9-20	1.552	.102	1.47	1.24	−.09		8.21	11.81	8.09	.34	.030								
	1.96	.5829	13-24	1.558	.102	1.46	1.53	−.08		8.51	12.09	8.64	.27	.024								
(c) Aerodynamic Facility, CO_2																						
1042	12.36	.8123	1-16	1.606	.132	1.41	−3.18	−.30	.1792	10.30	9.96	39.84	1.373	.055	2.0318	.1366	.02699	.6310	20.9001	.0213	7.65	3.34
1043	11.66	.7673	1-16	1.578	.125	1.33	−4.05	−.33	.1796	11.52	12.24	7.29	1.056	.022	2.0320	.1372	.02696	.6260	21.0150	.0212	7.97	3.15
1044	11.29	.7439	2-14	1.586	.130	1.48	−3.20	−.30	.1796	12.42	10.21	2.47	1.499	.030	2.0307	.1357	.02678	.6270	20.8976	.0214	8.13	3.04
1045	11.66	.7712	2-14	1.577	.125	1.27	.46	−.12	.1801	11.96	11.03	4.73	1.848	.040	2.0318	.1366	.02720	.6320	20.7349	.0214	7.70	3.14
1046	11.74	.7791	1-14	1.558	.122	1.37	1.27	−.08	.1805	12.52	15.08	5.06	1.415	.047	2.0318	.1357	.02666	.6260	21.0105	.0216	6.84	3.16
1047	11.65	.7736	1-14	1.589	.101	1.62	2.92	−.01	.1810	9.93	5.83	9.72	1.050	.046	2.0300	.1367	.02685	.6290	20.9730	.0214	8.77	3.14
1048	11.72	.7809	2-14	1.589	.134	1.46	−6.12	−.44	.1812	11.27	9.10	227.50	.808	.037	2.0297	.1359	.02666	.6250	20.9951	.0216	8.05	3.15

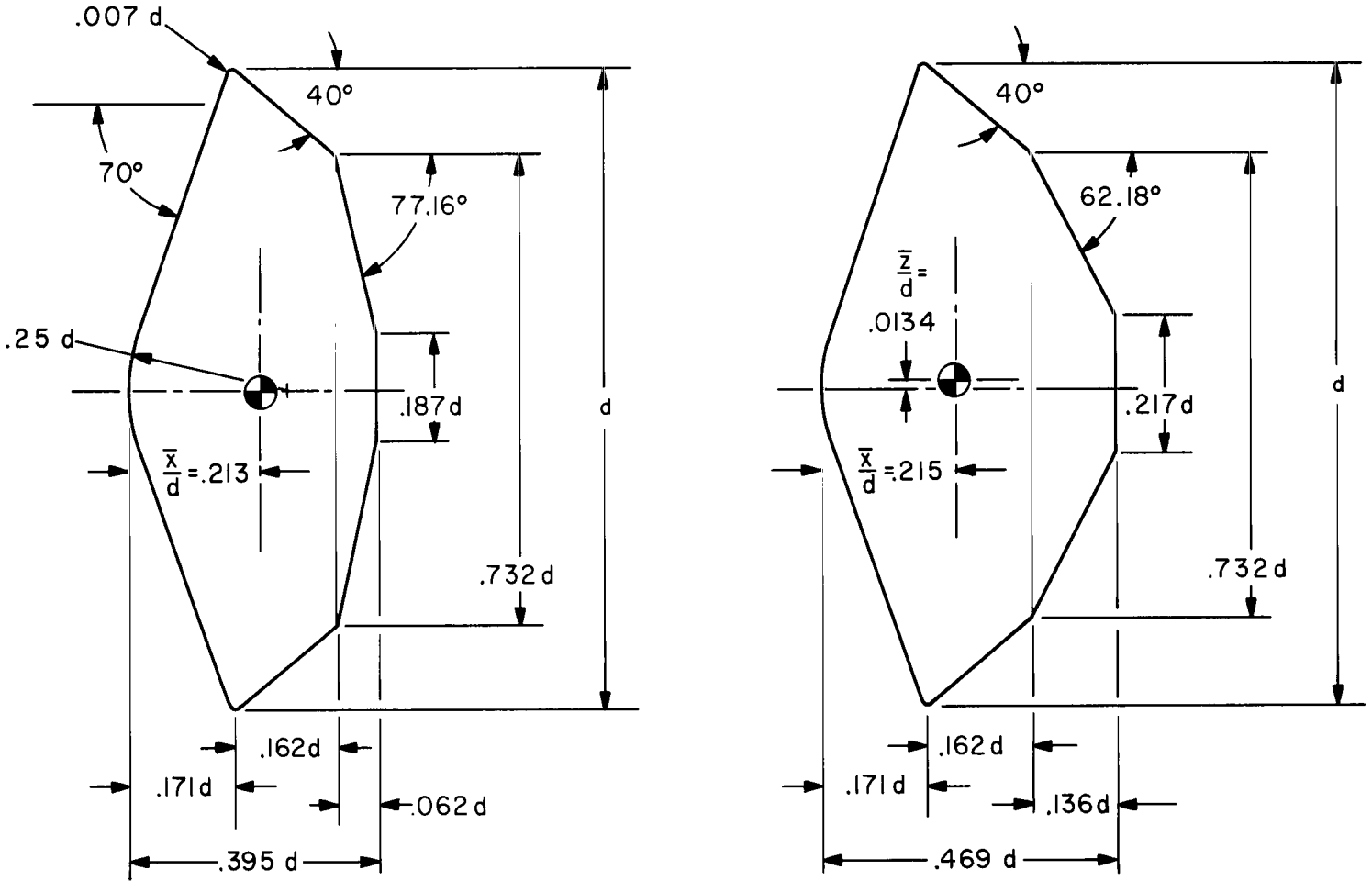

Note: These two models are identical in shape from the nose to a point .333 d. aft of the nose

(a) Homogeneous model.

Figure 1.– Model configurations.

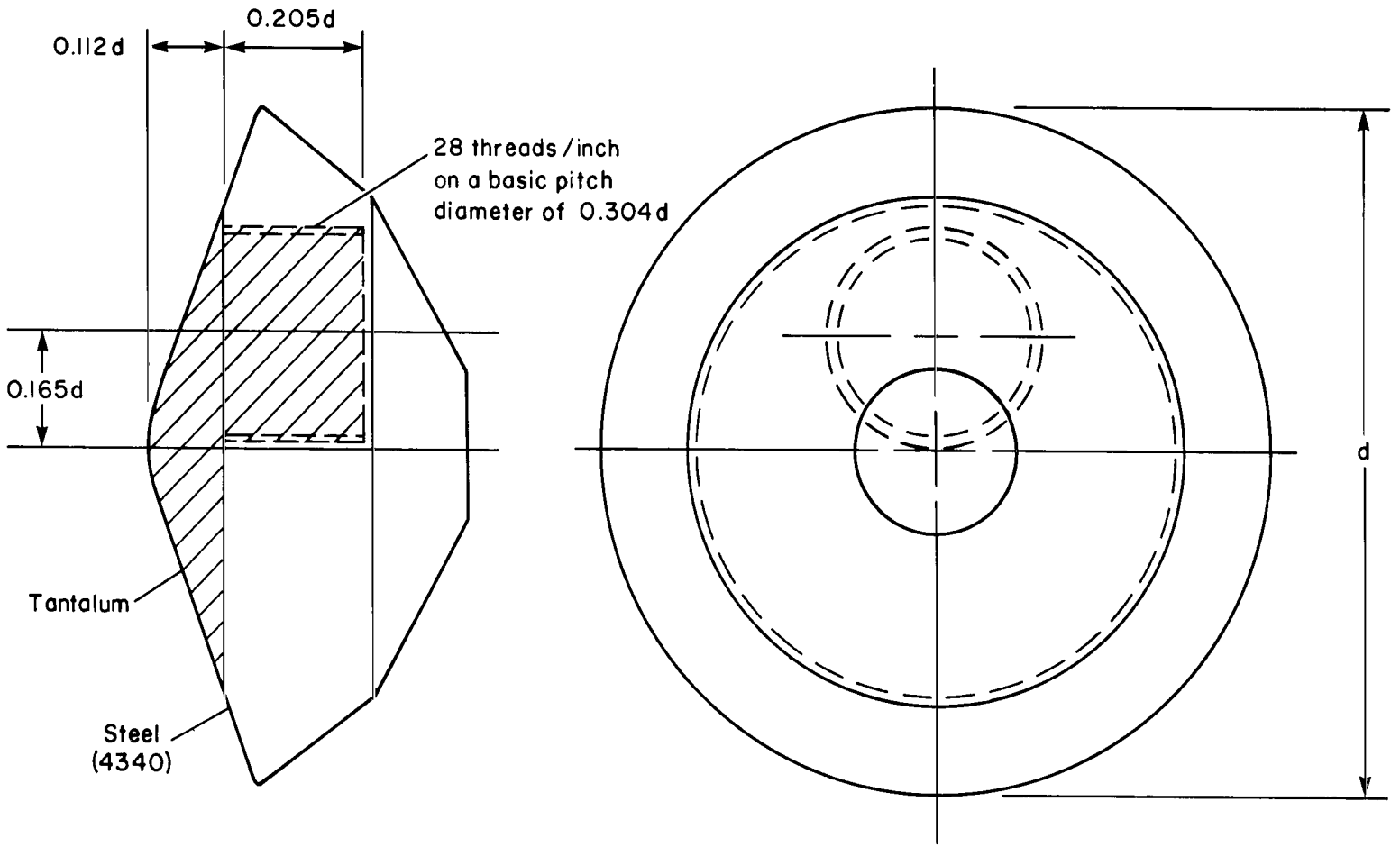

(b) Bimetallic model.

Figure 1.— Concluded.

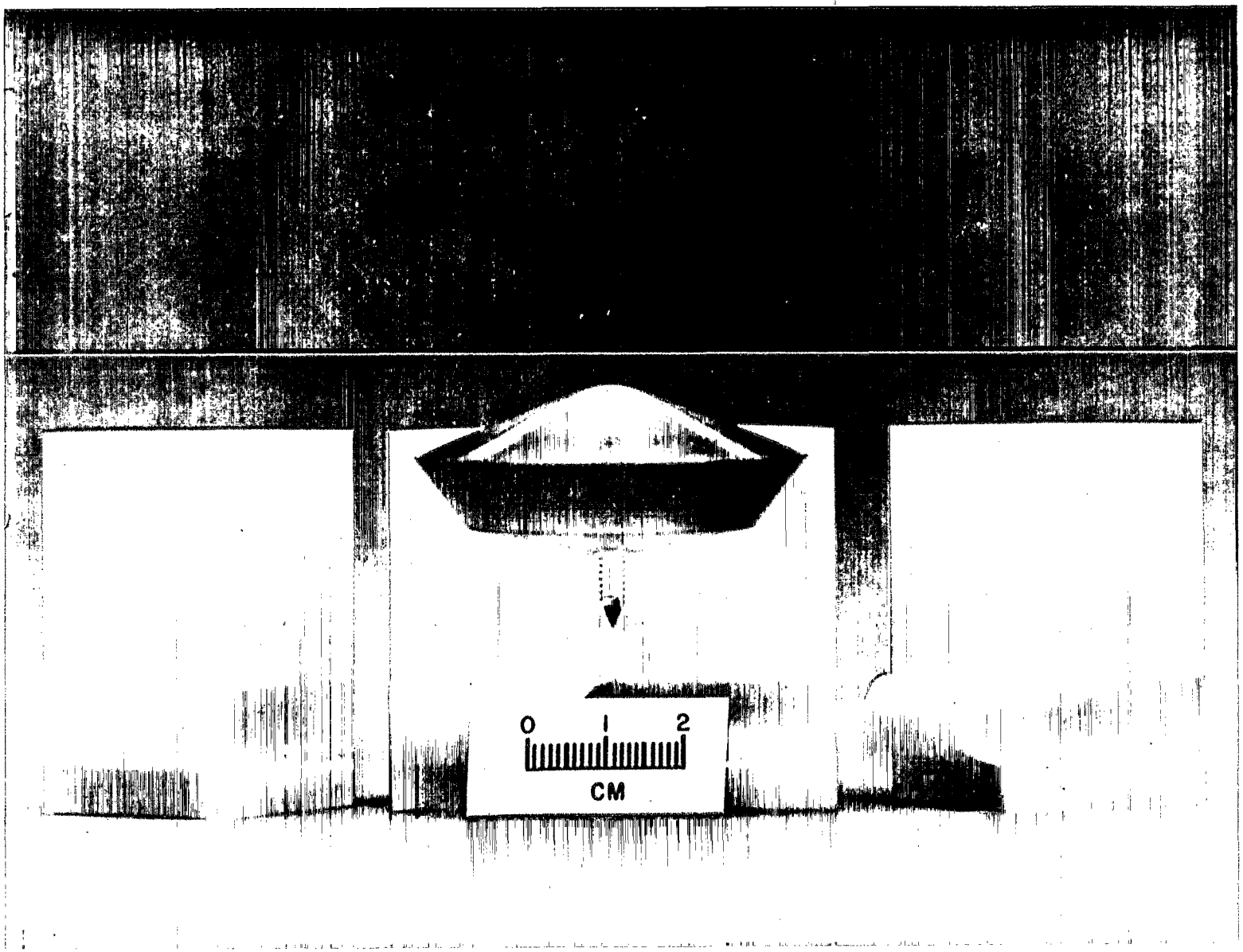

Figure 2.– Typical model and sabot combination.

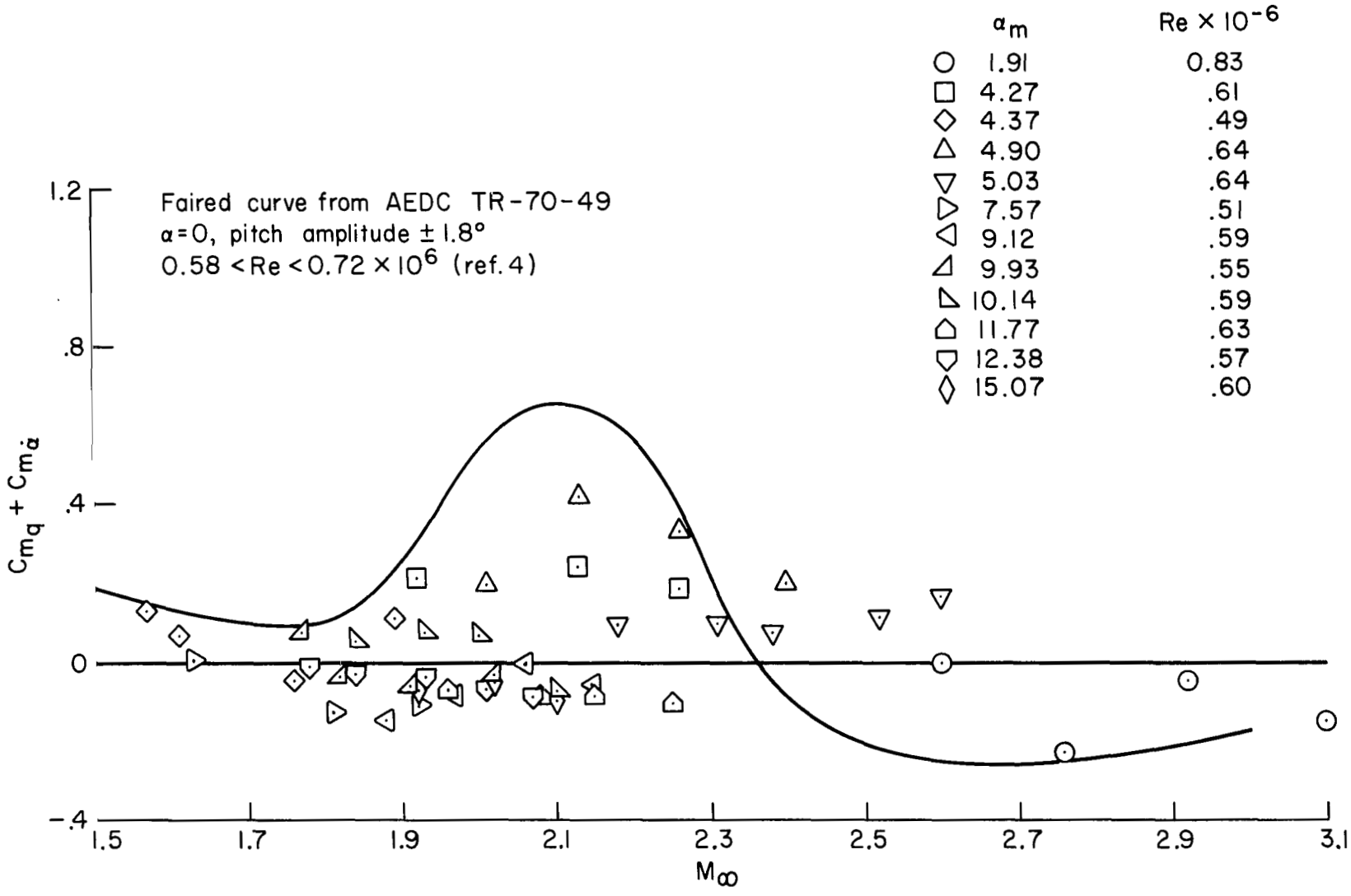

Figure 3.– Variation of the dynamic stability ($C_{m_q} + C_{m_{\dot{\alpha}}}$) with Mach number for model A in air.

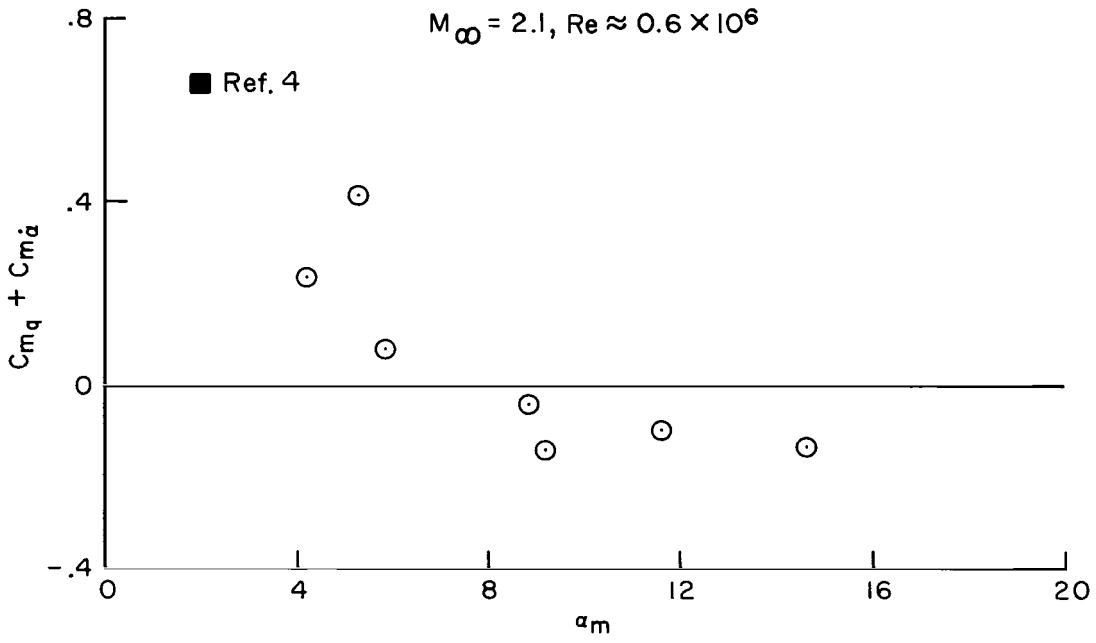

Figure 4.– Effect of pitch amplitude on the dynamic stability ($C_{m_q} + C_{m_{\dot{\alpha}}}$) of model A in air.

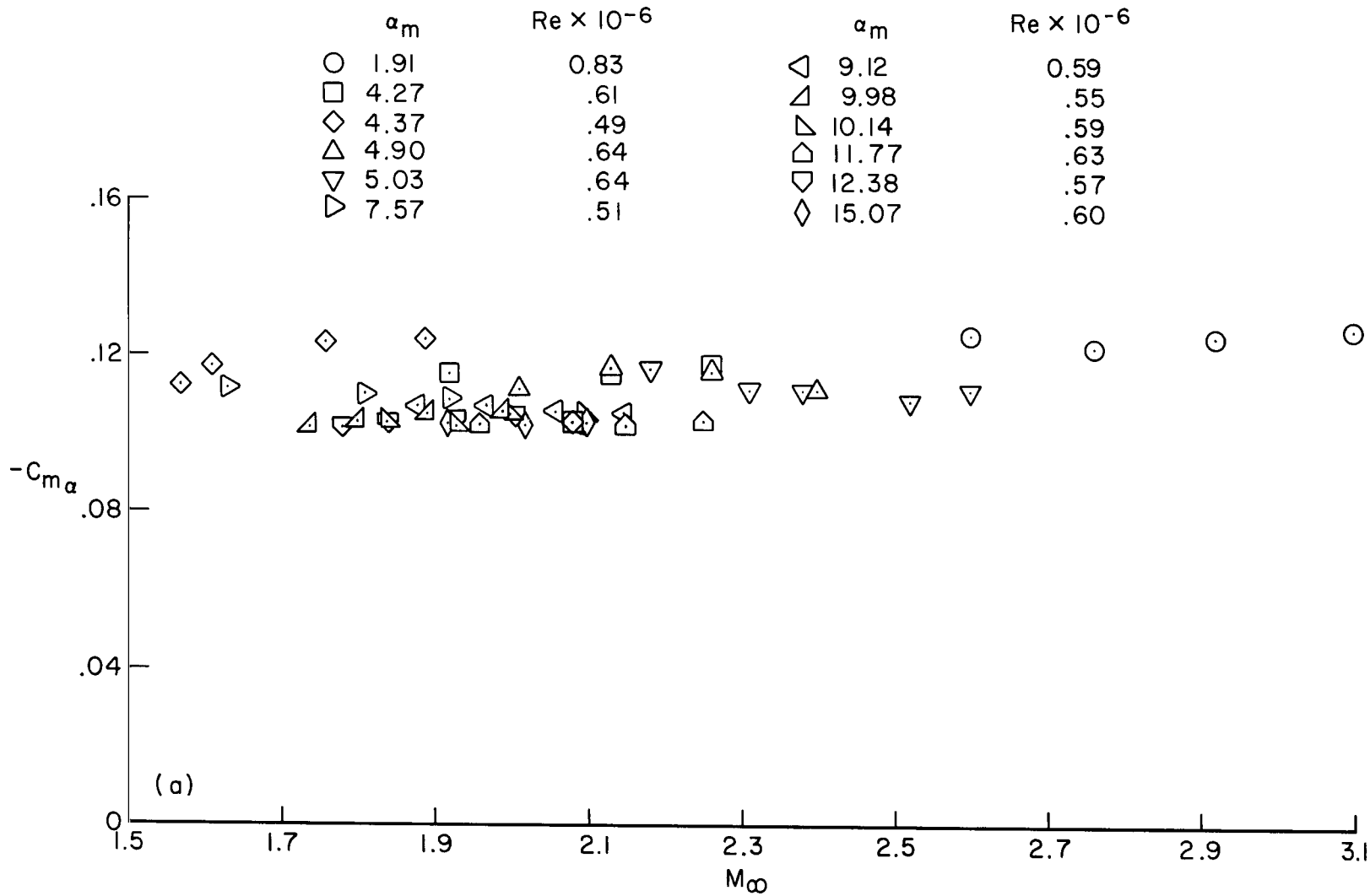

(a) C_{m_α} vs M_∞.

Figure 5.– Static stability (C_{m_α}) for model A in air.

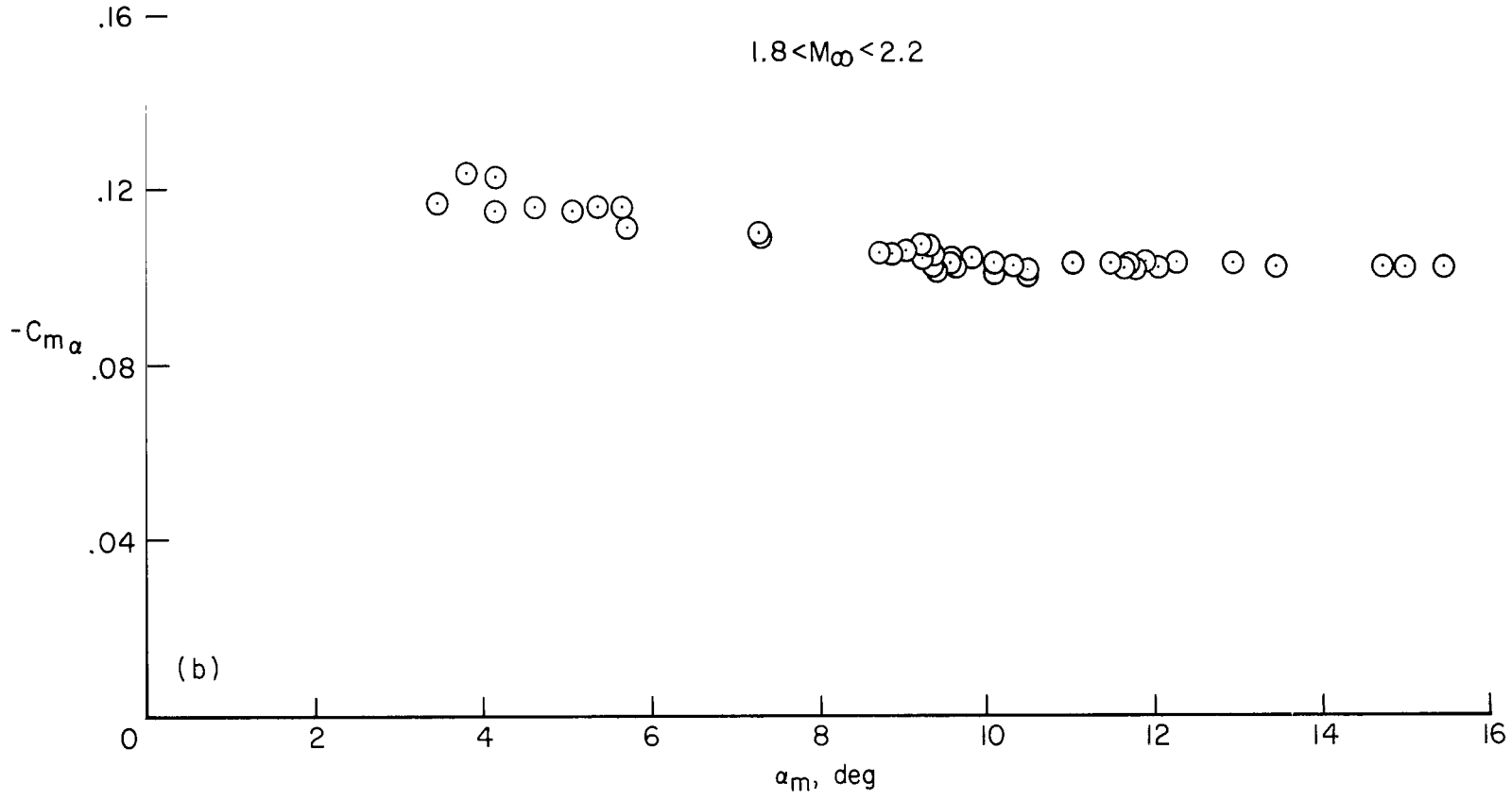

(b) C_{m_α} vs α_m.

Figure 5.– Concluded.

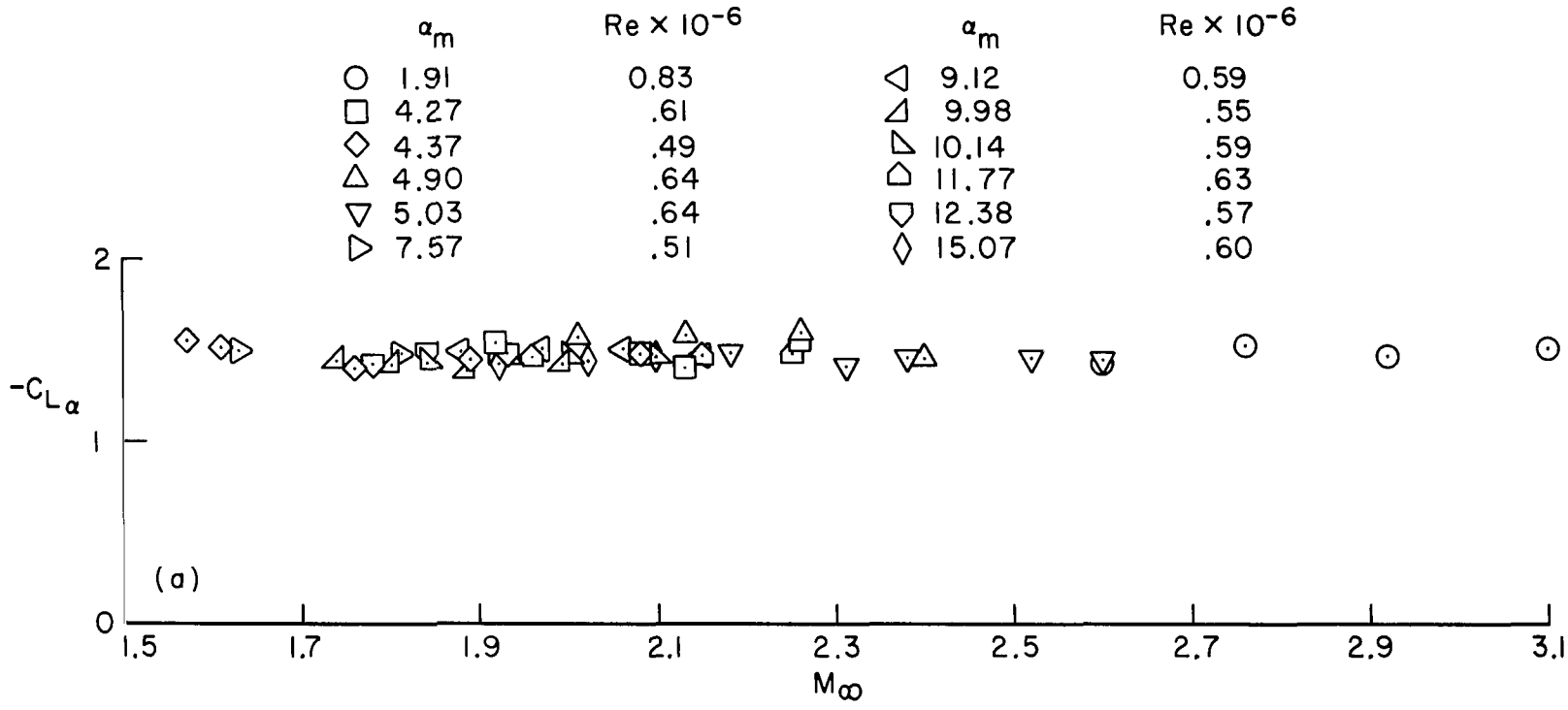

(a) C_{L_α} vs M_∞.

Figure 6.– Lift-curve slope (C_{L_α}) for model A in air.

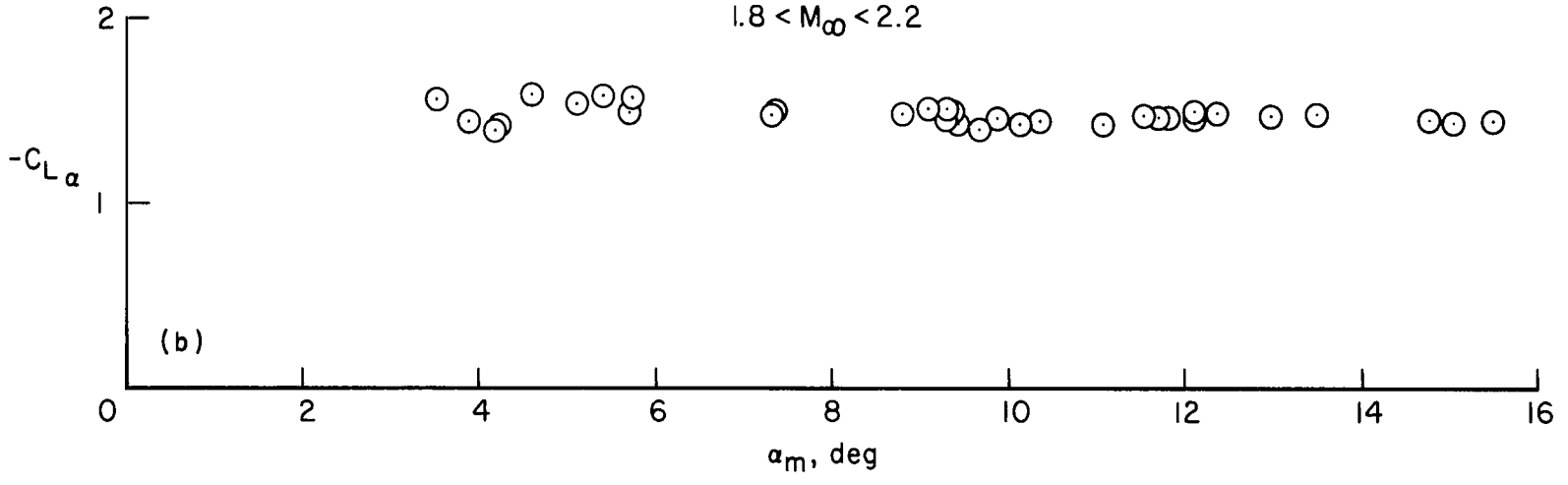

(b) C_{L_α} vs α_m.

Figure 6.– Concluded.

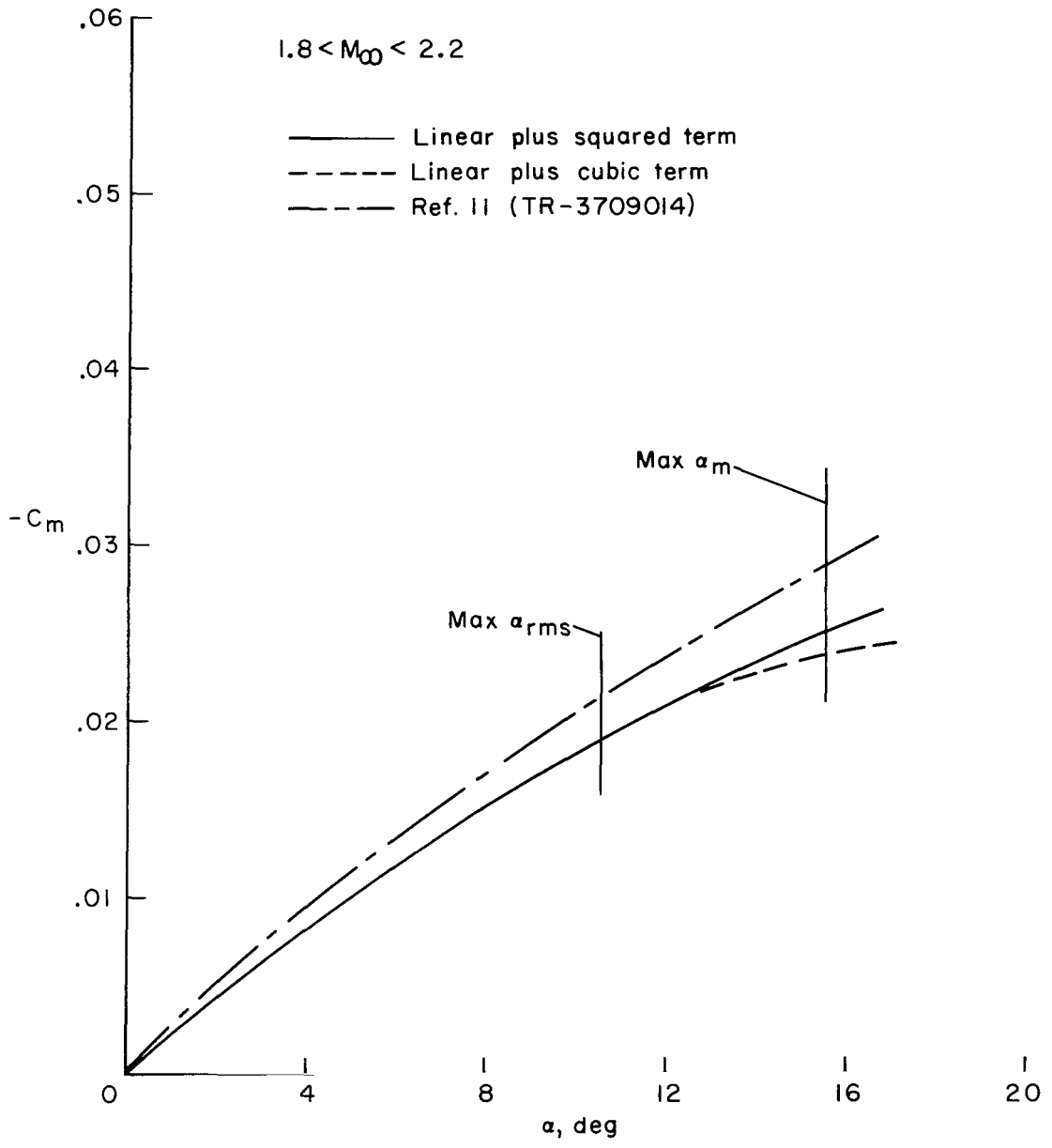

Figure 7.– Variation of the pitching-moment coefficient with angle of attack for model A in air.

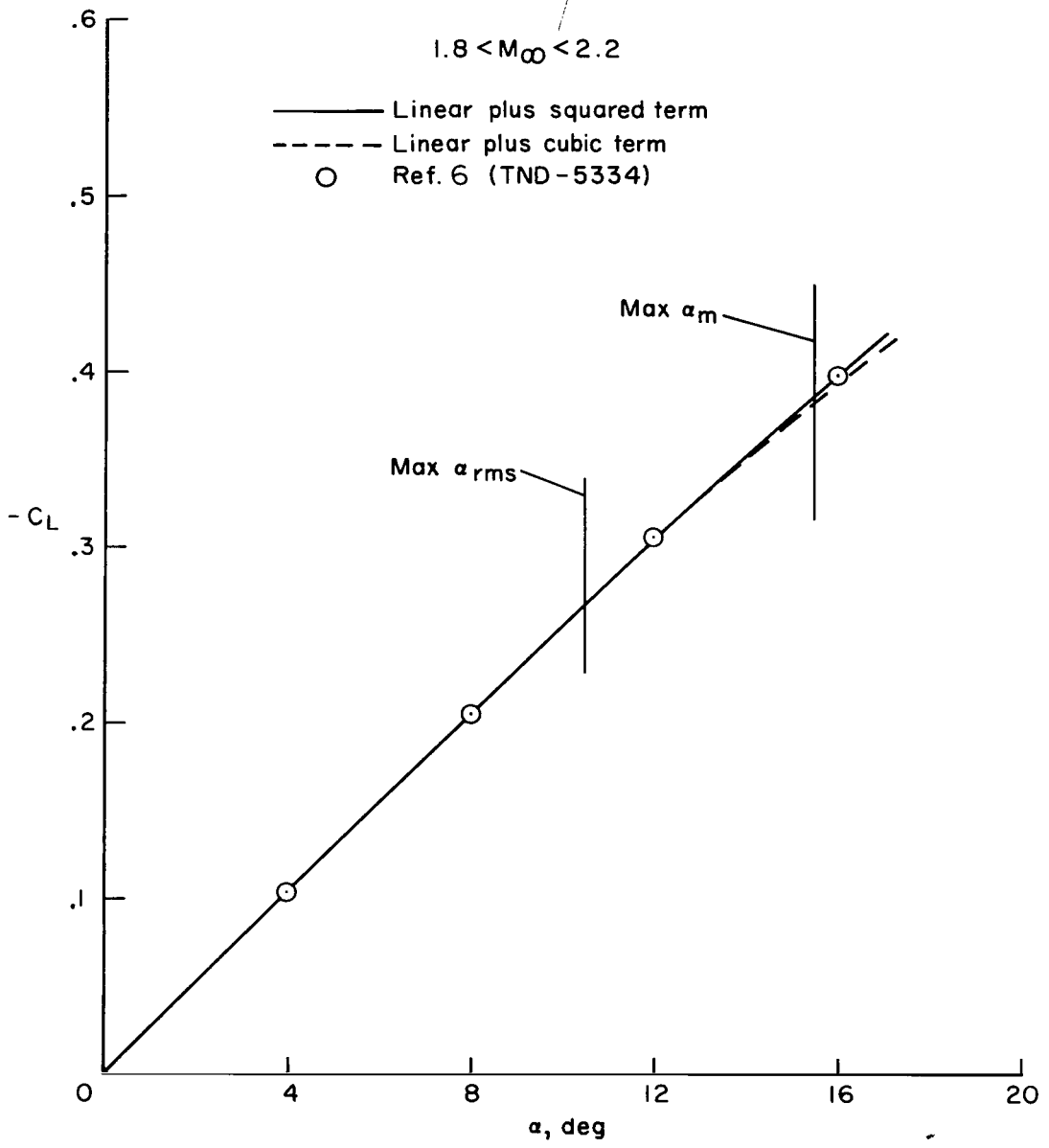

Figure 8.– Variation of the lift coefficient with angle of attack for model A in air.

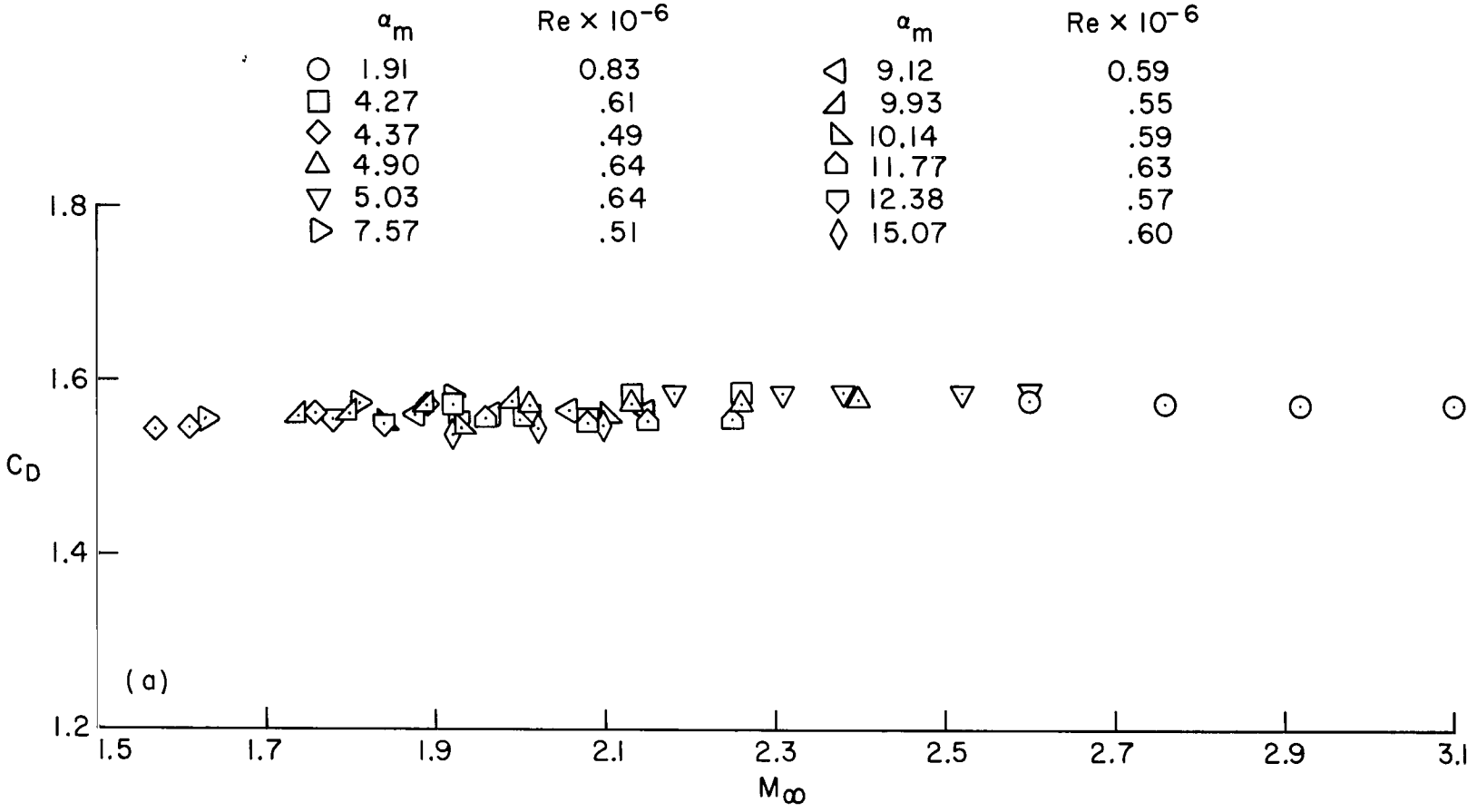

(a) C_D vs M_∞.

Figure 9.– Drag coefficient for model A in air.

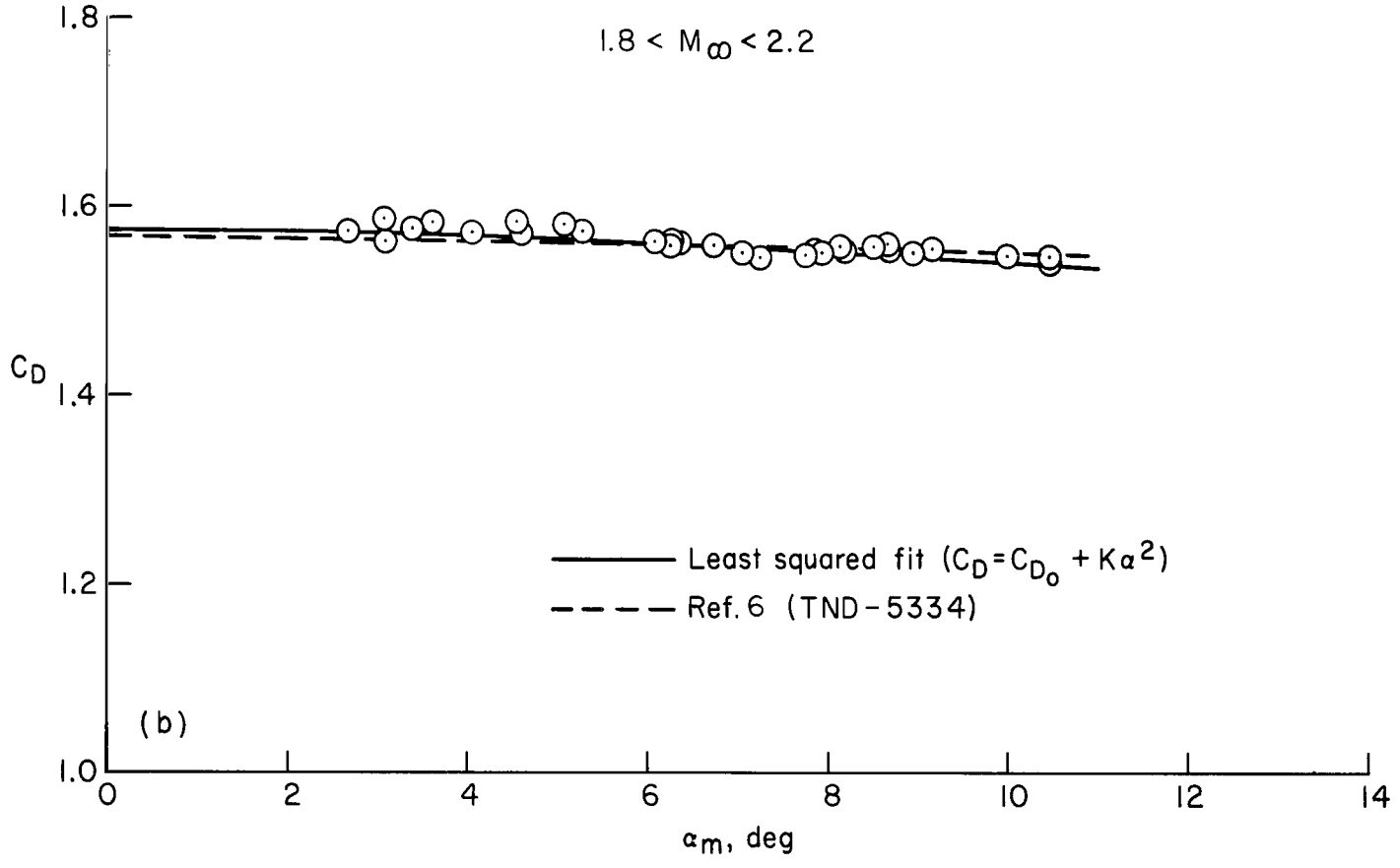

(b) C_D vs α_{rms}.

Figure 9.– Concluded.

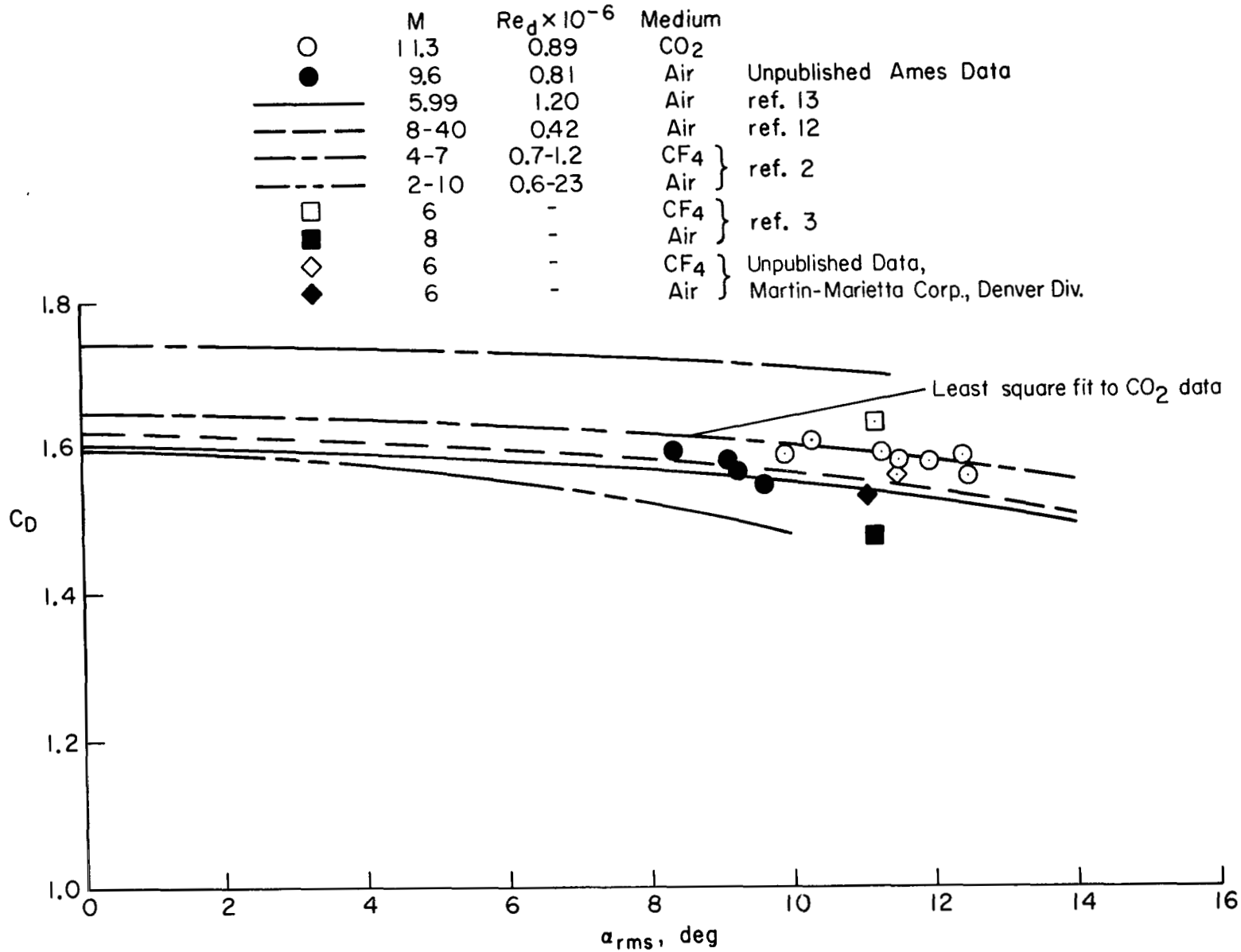

Figure 10.– Variation of the drag coefficient with angle of attack for model B in CO_2.

NATIONAL AERONAUTICS AND SPACE ADMINISTRATION
WASHINGTON, D.C. 20546

OFFICIAL BUSINESS
PENALTY FOR PRIVATE USE $300

SPECIAL FOURTH-CLASS RATE
BOOK

POSTAGE AND FEES PAID
NATIONAL AERONAUTICS AND
SPACE ADMINISTRATION
451

U.S.MAIL

571 001 C1 U A 750523 S00903DS
DEPT OF THE AIR FORCE
AF WEAPONS LABORATORY
ATTN: TECHNICAL LIBRARY (SUL)
KIRTLAND AFB NM 87117

POSTMASTER : If Undeliverable (Section 158 Postal Manual) Do Not Return

"The aeronautical and space activities of the United States shall be conducted so as to contribute . . . to the expansion of human knowledge of phenomena in the atmosphere and space. The Administration shall provide for the widest practicable and appropriate dissemination of information concerning its activities and the results thereof."

—NATIONAL AERONAUTICS AND SPACE ACT OF 1958

NASA SCIENTIFIC AND TECHNICAL PUBLICATIONS

TECHNICAL REPORTS: Scientific and technical information considered important, complete, and a lasting contribution to existing knowledge.

TECHNICAL NOTES: Information less broad in scope but nevertheless of importance as a contribution to existing knowledge.

TECHNICAL MEMORANDUMS: Information receiving limited distribution because of preliminary data, security classification, or other reasons. Also includes conference proceedings with either limited or unlimited distribution.

CONTRACTOR REPORTS: Scientific and technical information generated under a NASA contract or grant and considered an important contribution to existing knowledge.

TECHNICAL TRANSLATIONS: Information published in a foreign language considered to merit NASA distribution in English.

SPECIAL PUBLICATIONS: Information derived from or of value to NASA activities. Publications include final reports of major projects, monographs, data compilations, handbooks, sourcebooks, and special bibliographies.

TECHNOLOGY UTILIZATION PUBLICATIONS: Information on technology used by NASA that may be of particular interest in commercial and other non-aerospace applications. Publications include Tech Briefs, Technology Utilization Reports and Technology Surveys.

Details on the availability of these publications may be obtained from:

SCIENTIFIC AND TECHNICAL INFORMATION OFFICE

NATIONAL AERONAUTICS AND SPACE ADMINISTRATION

Washington, D.C. 20546